Science and Technology Indonesia
e-ISSN:2580-4391 *p*-ISSN:2580-4405
Vol. 10, No. 4, October 2025

Research Paper

Assessing Thermic Degradation for Yttrium–aluminum Precursive Agents Applied to YAG Phosphor Samples

Nguyen Thi Phuong Loan[1], Nguyen Doan Quoc Anh[2*], Phan Thi Minh Man[2], Hsiao-Yi Lee[3]

[1]*Faculty of Fundamental 2, Posts and Telecommunications Institute of Technology, Ho Chi Minh City, 70000, Vietnam*
[2]*Faculty of Electrical and Electronics Engineering, Ton Duc Thang University, Ho Chi Minh City, 70000, Vietnam*
[3]*Department of Electrical Engineering, National Kaohsiung University of Sciences and Technology, Kaohsiung City, 807618, Taiwan*
*__Corresponding author__: nguyendoanquocanh@tdtu.edu.vn

Abstract
Several forms of precursive agents were made via the soggy chemical approach, beginning with yttrium–europium–aluminum nitrate (YEAN) compound as well as disparate precipitants, comprising urea, oxalic acid, as well as ammonium carbonate. The precursive agents were heat-treated within nitrogen aerosphere for acquiring $Y_3Al_5O_{12}:Eu^{3+}$ featuring garnet formation YAG:Eu. Procedures employed for thermic degradation as well as constitution for precursive agents were validated via thermic assessment as well as FTIR spectroscopic assessment. Relationship among thermic degradation stages, as well as gaseous constitution developed throughout thermic procedure was identified via the merger between thermic assessment as well as FTIR. Ultimately, the disparate constitution for precursive agents signifies the luminescent attributes for matching phosphor samples. Urea as well as ammonium carbonate generate YAG samples featuring garnet formation as well as certain red discharge. Regarding oxalic acid, the precipitant yields an ununiform sample featuring yttrium oxide in the form non-pure stage. Said sample would be a merger between $Y_2O_3:Eu^{3+}$, $Y_4Al_2O_9:Eu^{3+}$, as well as $Y_3Al_5O_{12}:Eu^{3+}$, yielding greater discharge intenseness. When used in tandem with YAEN, AlAs was investigated for its particle size's effect on optical properties, such as scattering coefficient, YAG:Ce concentration, correlated color temperature (CCT), chroma aberration, lumen, and color rendition. It was found out 19 wt.% would be the most optimal particle size when all of these properties are taken into account.

Keywords
$KBaYSi_2O_7:Bi^{3+}$, YAG:Ce^{3+}, LEDs, Lumen Output, Color Quality

Received: 25 April 2025, Accepted: 14 August 2025
https://doi.org/10.26554/sti.2025.10.4.1209-1214

1. INTRODUCTION

Non-organic phosphor samples see copious research as they would be applicable to illumination techniques as well as manufacturing better displaying apparatuses including illuminating diode unit (LED), three-chroma fluorescent lights, field discharge display, etc. When it comes to augmenting brightness as well as resolution for such apparatuses, creating phosphor samples featuring significant proficiency, regulated granule form as well as magnitude would be compulsory (Thuy et al., 2025; Rianjanu et al., 2025).

YAG integrated with disparate rare-earth elements including Sm, Tb, Eu and so on, would be among the optimal substances employed for disparate uses for having greater mechanical consistency, small thermic extension, small phonic penalties as well as desirable optic attributes (Sagadevan et al., 2023). For instance, integrating Nd^{3+} as well as Ce^{3+} into YAG helps create colorant laser as well as novel illumination apparatuses. Triggering YAG via Eu^{3+} yields powders or narrow sheets employed for cathode beam as well as field discharge apparatuses. Crucial criterion that yields desirable proficiency for said apparatuses involves creating hyperfine phosphor granules featuring significant discharge intenseness (Esmerio et al., 2022; Hadi et al., 2025). The synthesizing procedure for YAG samples is conducted through disparate approaches including precipitance, sol-gel, ignition, as well as sprinkle pyrolysis. The study herein concerns creating YAG:Eu sampling units via the soggy chemical approach accompanied by reactivity approach. Several precursive agent forms were made via the reactivity approach beginning with YEAN compound as well as disparate precipitants. The precursive agents were heat treated for acquiring YAG:Eu (Sagadevan et al., 2023).

The research herein concerns more thorough assessment for procedures occurring throughout thermic degradation for precursive agents (Novianti et al., 2022). As such, thermic assessment involving gaseous advancement assessment as well as

FTIR assessments were conducted. Additionally, our research validates the influence for precipitant upon formational as well as luminescent attributes for YAG samples (Leong et al., 2022). Furthermore, AlAs with disparate particle sizes was employed for assessing the particle size's influence on various optical attributes, including scattering coefficient, YAG:Ce concentration, correlated color temperature (CCT), chroma aberration, lumen and color rendition. A particle size of 19 wt.% is considered the most balanced choice for all of these attributes. As of now, data on utilizing advanced gaseous is limited, and as such, the feasible activities manifesting throughout the degradation for precursive agents applied to creating YAG samples.

Compared to an earlier study on utilizing $Sr_8ZnSc(PO_4)_7$:Eu^{2+} and AlAs to enhance scattering (study A), AlAs integrated into YEAN of the study herein yields similar performance in color rendition (Cong and Anh, 2025). However, its influence on scattering as linear and inversely proportional as study A, while CCT variance is also far less volatile. It is worth noting that the lumen in this case is inversely proportional to AlAs particle size, as opposed to study A, meaning that YEAN does not benefit lumen when AlAs particle size is huge. Meanwhile, in comparison to another study on using $KBaYSi_2O_7$:Bi^{3+},Eu^{3+} phosphor for boosting color quality in WLED (study B), the YEAN sample and AlAs of this study produce far more consistent CRI, YAG:Ce concentration and CCT variance (Loan et al., 2024). However, the CQS and lumen outputs always decrease with bigger AlAs particle sizes of this study, unlike study B which reports CQS and lumen increasing with higher particle sizes of $KBaYSi_2O_7$:Bi^{3+},Eu^{3+} phosphor. As such, compared to its counterparts, YEAN sample generally only benefits optical properties if the particle size is smaller.

2. EXPERIMENTAL SECTION

2.1 Materials

YAG:Eu samples were made via the soggy chemical approach while administrating reacting agents through disparate precipitant forms of precipitation substances including urea corresponding to sample A, ammonium carbonate (AC) corresponding to sample B as well as oxalic acid (OA) corresponding to sample C. Yttrium- europium-aluminum (YEA) precursive agents were made using $Y(NO_3)_3{\cdot}5H_2O$, $Al(NO_3)_3{\cdot}9H_2O$, $Eu(NO_3)_3{\cdot}5H_2O$ for providing metal ions as well as urea, ammonium carbonate, oxalic acid dihydrate for providing anions (Dang et al., 2021; That and Anh, 2021). Said commercial materials required no further purification. TiO_2 and YAG:Ce were obtained with high purity.

2.2 Procedure

The synthesizing procedure for YAG:Eu was conducted throughout two periods. The initial period involved synthesizing YEA precursive agents via precipitating process involving equivalent quantities for YEAN compound accompanied by urea, ammonium carbonate, or oxalic acid concurrently administered unto weakened compound containing matching precipitant. The period posterior to precipitating for precursive agent lasted within one day, comprising aging, cleansing, centrifugal procedure as well as desiccating. The final period for the approach involved thermic procedure for the precursive agents within N_2 aerosphere. The acquired samples were cleansed, desiccated then strained. The creation procedure for phosphor did not require ball-grinding (Li et al., 2019; Li et al., 2018).

2.3 Instrument and Analysis

Precursive agents underwent various examinations. Thermogravimetric as well as divergent thermic assessment was conducted via an analytic apparatus employed for thermogravimetry (TGA) (METTLER TOLEDO/SDTA851). Advanced gaseous assessment was conducted via a Nicolet 6700 FT-IR Spectrometric apparatus (Thermo Scientific) accompanied by one TGA component and HR Nicolet TGA Vapor stage database. Fourier-Transform infrared absorptivity spectroscopic assessment was conducted via the same spectrometric apparatus utilizing the KBr pilule approach. Exterior zone assessments were conducted via a TriStar II3020 apparatus (Micromeritics) featuring a decontaminating process within nitrogen flux. Scanning electronic microscopic assessment was conducted via a JSM 5510LV scanning electronic microscopic apparatus (JEOL) utilizing powdered samples daubed with Au. Attribute assessment for phosphor samples was conducted via X-ray diffraction using D8 Advance X-ray diffractometric apparatus (BRUKER) with Cu Kα radioactivity. Photoluminescent assessments were conducted via FP-6500 spectrofluorimetric apparatus (JASCO) utilizing WG 320 glass sifter (Limbu et al., 2020; Lissner and Urban, 2011).

3. RESULTS AND DISCUSSION

3.1 Thermic Degradation Stages and Gaseous Constitution Developed Throughout Thermic Procedure

For determining the impact from precipitants upon formations as well as photoluminescent attributes for YAG:Eu, several forms of YEA precursive agents were made via the soggy chemical approach, including sample A made via urea, sample B made via AC, as well as sample C made via OA. Posterior to thermic procedure for precursive agents, phosphor sampling units were acquired. The precursive agent constitution was identified via thermic assessment as well as spectroscopic assessment. Relationship among thermic degradation periods, proportion penalty as well as constitution for gaseous advancement throughout thermic procedure for precursive agents was validated via merging thermic assessment as well as FTIR approach (Liu et al., 2019a; Liu et al., 2019b).

The precursive agents' constitution was examined via thermic assessment as well as infrared spectroscopic assessment. The interaction among thermic degradation stages as well as gaseous constitution developed throughout thermic procedure was identified via the merger between thermic assessment as well as FTIR. The thermic assessment yields data concerning the alterations manifesting throughout the thermic processing. The DTA arches concerning the precursive agents made via disparate precipitative substances display thermic influences

for the primary stages. The degradation phases for sample C (OA) would be clearly displayed via pronounced endothermal apexes compared to B (AC) as well as A (urea) precursive agents. Said alterations may result from multiple activities including abolishment for assimilated water; abolishment for chemical-bound water in the case of samples A, B, C; degradation for oxalate-derived category in the case of sample C, degradation for elementary carbonate as well as nitrate compounds in the case of samples A, B; degradation for carbonate as well as oxycarbonate substances in the case of sample C.

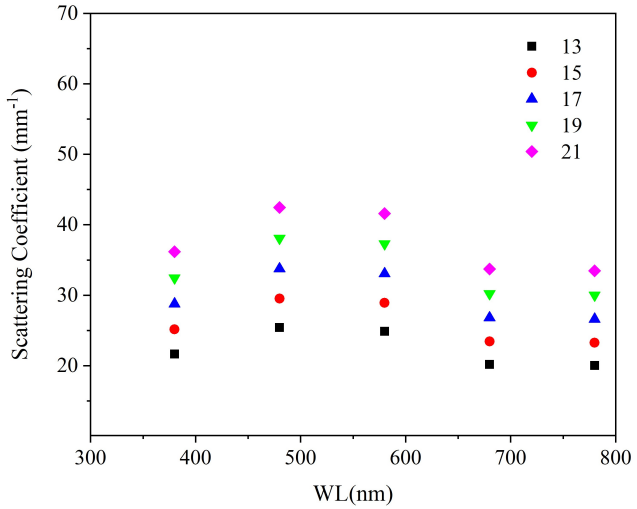

Figure 1. Relationship between Scattering Coefficient and Wavelength

Advanced gaseous assessment yields further data on the activities manifesting throughout the transmutation for the precursive agents to form matching phosphor samples. The primary degradation features a significant gaseous discharge manifesting under lower temperatures for samples A and B as well as greater temperatures for sample C. The primary gases advanced throughout the thermic processing for the precursive agents include CO_2, NH_3, water, N_2O, NO_2, and CO. The unleashed gases comprise ammonia for sample A; water for samples A, B, C; as well as CO_2 for samples A, B, C. The CO_2 abolishment under small heat levels signifies the degradation for hydroxide carbonate composites. The concurrent discharge for NH_3, CO_2, as well as water in the case of sample A signifies that composites featuring complicated constitution comprising ammonium hydroxide carbonate substances would be generated throughout the precipitating activity.

With the progress in thermic processing as well as the surge in heat level, every precursive agent concurrently unleash CO_2, as well as a tiny water quantity, resulting from the degradation for metal elementary carbonate substances. Ammonia remnants remain within sample A. Furthermore, novel bands manifest, resulting from the dinitrogen oxide discharge (metal nitrate degradation). As time passes, the distinctive absorptivity in water grows greater, surpassing CO_2, in the case of samples A and B. Based on said mechanism, the primary activity may be the degradation for metal hydroxide substances. NO_2 remnants remain within samples A and B. Under said phase, the degradation for metal nitrate substances is reaching its end. In the case of sample C (OA), a significant gaseous discharge primarily comprising CO_2 as well as CO manifests. Based on said mechanism, the primary element in sample B's precursive agent would be metal oxalate substances. Ammonia as well as water remnants can be perceived, indicating the degradation for tiny quantities of ammonium oxalate. Under high temperatures, every precursive agents abolish CO_2, resulting from carbonate degradation.

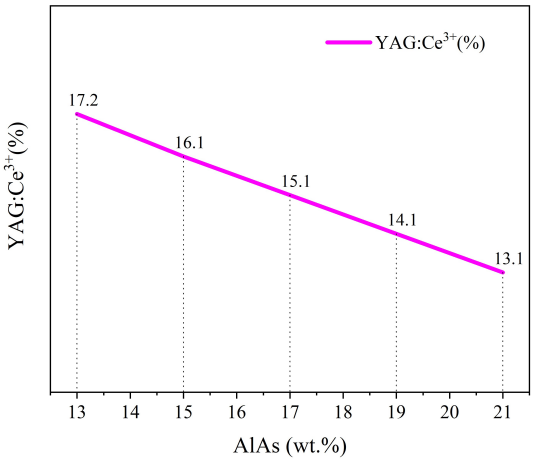

Figure 2. YAG:Ce Presence Interacting with Particle Size of AlAs

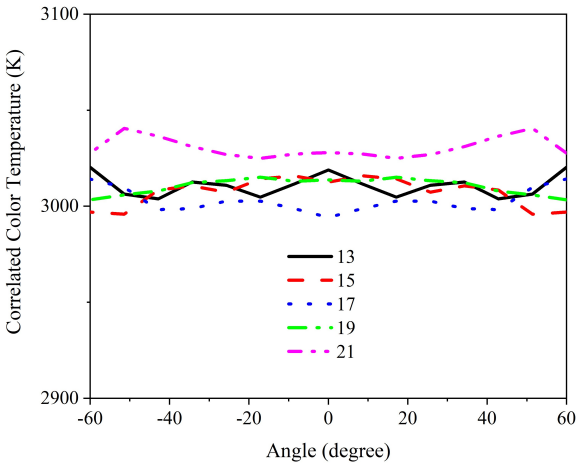

Figure 3. CCT Alteration Based on Particle Size

3.2 AlAs's Influence on Optical Properties

Due to its unique optical properties, including a high refractive index and favorable dispersion characteristics, AlAs is advantageous when used in conjunction with optical phosphor

materials in WLED devices. When integrated into phosphor sheets, AlAs grains may modify the interaction between light and materials. AlAs may serve as effective tiny dispersers that direct and scatter light produced by LED chips, enhancing light distribution and ensuring consistent lighting distribution. By modifying the AlAs dose in conjunction with other phosphor samples, one may effectively control optical characteristics like as color rendition, correlated color temperature (CCT), and luminous flux. In addition to dispersion, the use of AlAs with typical phosphor samples such as YAG:Ce may enhance chromatic rendition.

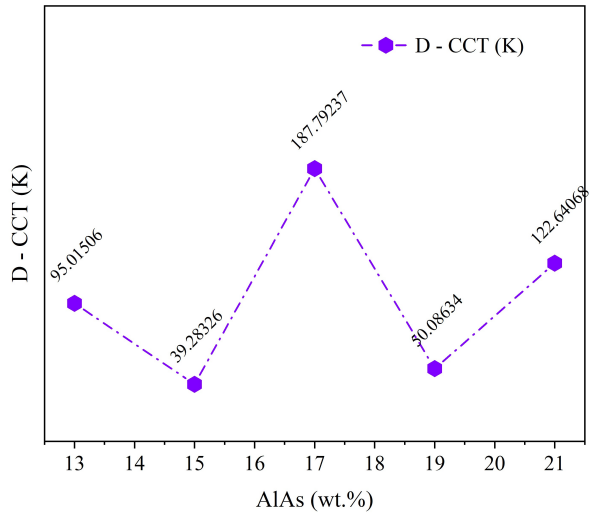

Figure 4. Variation in Hue Aberration under Alas Particle Size

Figure 1 features the changes of the scattering coefficients under different wavelengths. The scattering coefficient may assess optical performance in WLED devices by enhancing dispersion activities, hence improving consistency in light distribution and color quality. Nonetheless, excessive quantities of the specified element may diminish luminosity, since light would be inadequately contained or directed. The coefficient is directly proportional to the AlAs concentration, rising with higher levels of AlAs. When it comes to influence from wavelength, said coefficient shows a noticeable increase as the wavelength reaches 500 nm. Afterwards, it shows a slight abatement at 600 nm and a much greater abatement at 700 nm, which causes dispersion for the light produced by the blue chip to propagate and then more convert into rays at longer wavelengths. These changes appear to be the result of an inverse mechanism (Liu et al., 2012; Shi et al., 2023). Then, when the blue-ray dispersion in the front discharge surge with the blue-ray repeating absorptivity and rear-dispersion decreased, the luminescence will be increased. When the AlAs particle size increases, the YAG:Ce content must decrease in order to achieve this goal, which is demonstrated by Figure 2 exhibiting the YAG:Ce content being influenced by the particle size. When included into YAG:Ce phosphor sheets, AlAs enhances light dispersion due to its substantial refractive index. This dispersion enhances angle chroma consistency for produced light, guaranteeing visual uniformity across different viewing angles. As can be seen, the content falls as the particle size of BaF_2 escalates. The presence of AlAs requires careful monitoring, since excessive amounts reduce luminosity owing to a part of light being absorbed by phosphor sheets. Conversely, AlAs induces redshift in the discharge spectrum, modifying CCT levels in the WLED system, as seen in Figure 3. The particle size also affects CCT levels, as shown by Figure 3. Under all particle sizes, the CCT displays mostly small fluctuations with barely any significant changes. Under a particle size of 17 and 21 wt.%, the CCT shows the most noticeable fluctuations, but shows smallest fluctuations under 19 wt.%, indicating highest CCT consistency at this level of particle size. The CCT is at its lowest under particle size of 17 wt.%. In contrast, the CCT reaches its peak under the particle size of 21 wt.%.

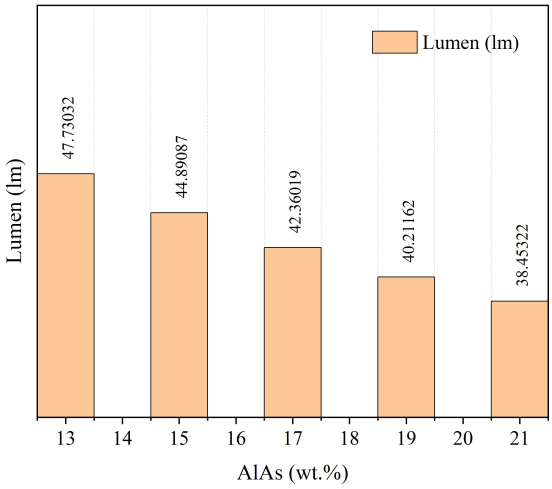

Figure 5. LED Lumen Generated Based on Alas Particle Size

The hue aberration shows fluctuations under various particle sizes, as demonstrated by Figure 4. Notably, the hue aberration shows a very significant decrease when the particle size reaches 19 wt.%. With greater particle sizes, however, it considerably surges. For the lumen in LED shown in Figure 5, it undergoes inverse changes, displaying a consistent abatement when the particle size surges. The maximum lumen is attained with the smallest particle size at 17 wt.%, suggesting that this particle size is optimal for achieving the desired lumen output. The observed changes may be the consequence of the difference in color allocation and the lower intensity of the blue discharge due to increased rear-dispersion and repeated absorptivity. It should be noted that as particle size increases, the phosphor sheet typically has a wider width, which lowers the energy of the whole spectrum. As a result, the lighting transmutation between blue and yellow or red-orange will be more pronounced. This indicates that the transmuted beam may participate in rear-reflection under extremely large particle sizes, which would reduce the luminous intensity and produce a higher CCT level (Tang et al., 2021; Anh and Lee, 2024).

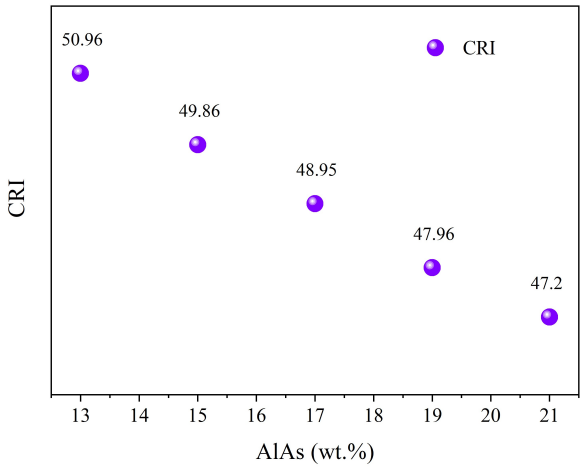

Figure 6. CRI Subject to Changes in AlAs Particle Size

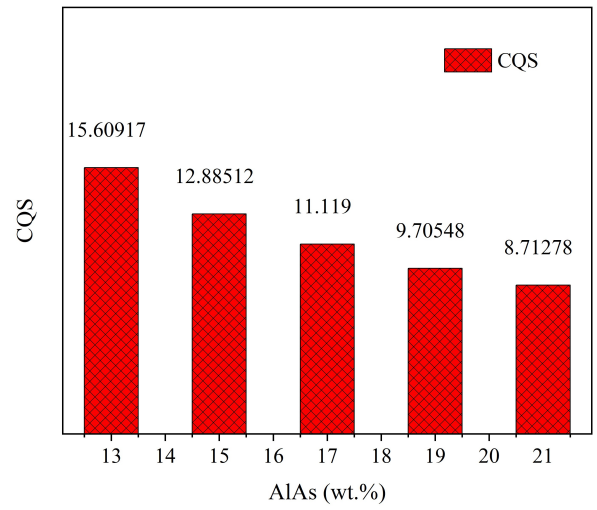

Figure 7. CQS Under Influence of AlAs Particle Size

The particle size has an impact on the WLED device's color generation output as well. In Figures 6 and 7, there are considerable declines for CRI and CQS as the particle size grows. The color difference between the orange-yellow, blue, and green components may be the cause of several crashes that have been seen. The reason for this discrepancy is that with large particle sizes, the increased dispersion produces more orange-yellow components since the discharge color of the rays often favors the orange-yellow zone. Therefore, excessive dispersion may result in lower CRI and CQS (Tung et al., 2024a; Tung et al., 2024b). If all aforementioned optical properties are taken into account, in addition to CRI and CQS, 19 wt.% would be the most optimal particle size.

Concerning the task of measuring hue quality, CRI would be considered the most common and the oldest index. In order to gauge hue quality, CRI assesses eight hue samples under testing illumination and natural illumination, then compares the conditions. CRI proves to be useful when it comes to assessing hue performance in illumination with wide spectrum. However, this index was developed well before the development of LED devices, and thus, is not suitable to apply on these devices. Using only the few hue samples from CRI, the desaturation resulted would be too much for appropriately assess chromatic output from LED devices (Cong et al., 2024; Le et al., 2024). CQS was proposed to remedy this weakness, by assessing fifteen hue samples, and thus is capable of yielding more authentic hue assessments. In addition to increased hue samples, CQS also include other factors: individual's taste and hue disparity. As a newer index proposed in a modern era, CQS would be a more fitting index for examining the hue performance in modern devices like LED (Anh and Lee, 2024).

4. CONCLUSIONS

YEA precursive agents were subject to precipitation via urea, ammonium carbonate as well as oxalic acid by utilizing soggy chemical approach and concurrently administering reacting agents. The thermic assessment involving gaseous assessment validated the activities manifesting throughout the thermic procedure for precursive agents applied to the synthesizing procedure for YAG:Eu samples. The primary degradation period for precursive agents leads to a significant gaseous discharge. Urea as well as ammonium carbonate yield YAG samples featuring garnet formation as well as distinctive discharge. Oxalic acid yields an ununiform phosphor featuring greater discharge intenseness. In addition to YAEN, AlAs was investigated for its particle size's effect on optical properties, such as scattering coefficient, YAG:Ce concentration, correlated color temperature (CCT), chroma aberration, lumen and color rendition. It was found out 19 wt.% would be the most optimal particle size when all of these properties are taken into account.

5. ACKNOWLEDGEMENT

The authors wishes to express their gratitude to the Posts and Telecommunications Institute of Technology, Vietnam, for financial support for this research.

REFERENCES

Anh, N. D. Q. and H. Y. Lee (2024). Titanium Dioxide in Vanadate Red Phosphor Compound for Conventional White Light Emitting Diodes. *Optoelectronics and Advanced Materials - Rapid Communications*, **18**(9–10); 480–484

Cong, P. H. and N. D. Q. Anh (2025). Augmenting Chroma Performance for WLED Employing $Sr_8ZnSc(PO_4)_7:Eu^{2+}$@AlAs as a Scattering-Enhancing Substance. *Science & Technology Indonesia*, **10**(2); 467–472

Cong, P. H., L. X. Thuy, N. T. P. Loan, H. Y. Lee, and N. D. Q. Anh (2024). ZnO-Doped Yellow Phosphor Compound for Enhancing Phosphor-Conversion Layer's Performance in White LEDs. *Optoelectronics and Advanced Materials - Rapid Communications*, **18**(7–8); 389–395

Dang, N. H. S., D. M. T. Nguyen, T. P. L. Nguyen, D. Q. A. Nguyen, and H.-Y. Lee (2021). Enhance WLEDs Performance with Additional Phosphor Materials in Multi-Layer Remote Structure. *Journal of Advanced Engineering and Computation*, **5**(3); 167

Esmerio, C. L., C. R. Rojas, J. A. Rocha, E. L. Medina, F. R. Brito, E. C. García, R. M. Martinez, M. A. Frutis, and M. G. Hipólito (2022). Study of the Electrical, Optical and Morphological Properties in Submicron and Microstructured ZnO Thin Films Obtained by Spin Coating and Chemical Bath Deposition. *Science & Technology Indonesia*, **7**(3); 291–302

Hadi, D. S., H. Wafda, A. P. A. Mustari, V. Trisnawan, N. Widiawati, F. Miftasani, and D. H. Prajitno (2025). Corrosion Behavior of Modified F/M Steel with Ti and Dispersed Oxides: Y_2O_3 and ZrO_2 Under High Temperature in Static Liquid Lead. *Science & Technology Indonesia*, **10**(3); 877–888

Le, P. X., N. D. Q. Anh, and H. Y. Lee (2024). Regulating the White LED Properties with Different AlAs Particle Sizes. *Optoelectronics and Advanced Materials - Rapid Communications*, **18**(9–10); 485–489

Leong, C. Y., H. L. Teh, M. C. Chen, and S. L. Lee (2022). Effect of Synthesis Methods on Properties of Copper Oxide Doped Titanium Dioxide Photocatalyst in Dye Photodegradation of Rhodamine B. *Science & Technology Indonesia*, **7**(1); 91–97

Li, H., R. Pang, Y. Luo, H. Wu, S. Zhang, L. Jiang, D. Li, C. Li, and H. Zhang (2019). Structural Micromodulation on Bi^{3+}-Doped $Ba_2Ga_2GeO_7$ Phosphor with Considerable Tunability of the Defect-Oriented Optical Properties. *ACS Applied Electronic Materials*, **1**(2); 229–237

Li, Z., Y. Tang, J. Li, C. Wu, X. Ding, and B. Yu (2018). High Color Uniformity of White Light-Emitting Diodes Using Chip-Scaled Package. *IEEE Photonics Technology Letters*, **30**(11); 989–992

Limbu, S., L. R. Singh, and G. S. Okram (2020). The Effect of Lithium on Structural and Luminescence Performance of Tunable Light-Emitting Nanophosphors for White LEDs. *RSC Advances*, **10**(59); 35619–35635

Lissner, I. and P. Urban (2011). Toward a Unified Color Space for Perception-Based Image Processing. *IEEE Transactions on Image Processing*, **21**(3); 1153–1168

Liu, D., P. Dang, X. Yun, G. Li, H. Lian, and J. Lin (2019a). Luminescence Color Tuning and Energy Transfer Properties in $(Sr,Ba)_2LaGaO_5$:Bi^{3+},Eu^{3+} Solid Solution Phosphors: Realization of Single-Phased White Emission for WLEDs. *Journal of Materials Chemistry C*, **7**(43); 13536–13547

Liu, S., Y. Liang, Y. Zhu, H. Li, J. Chen, and S. Wang (2019b). The Exploration of Structure Evolution and Photoluminescence Property in $Ca_9Al_{1-Y}(PO_4)_7$:Eu^{2+} Solid Solution Phosphors via the Construction of Bi-Directional Relationships. *Journal of Alloys and Compounds*, **785**; 573–583

Liu, Z.-Y., C. Li, B.-H. Yu, Y.-H. Wang, and H.-B. Niu (2012). Effects of YAG:Ce Phosphor Particle Size on Luminous Flux and Angular Color Uniformity of Phosphor-Converted White LEDs. *Journal of Display Technology*, **8**(6); 329–335

Loan, N. T. P., L. X. Thuy, N. L. Thai, H. Y. Lee, and P. H. Cong (2024). Application of $KBaYSi_2O_7$:Bi^{3+},Eu^{3+} Phosphor for White Light-Emitting Diodes with Excellent Color Quality. *Science & Technology Indonesia*, **9**(3); 756–765

Novianti, D. R., F. Haikal, U. A. Rouf, A. Hardian, and A. Prasetyo (2022). Synthesis and Characterization of Fe-Doped $CaTiO_3$ Polyhedra Prepared by Molten NaCl Salt. *Science & Technology Indonesia*, **7**(1); 17–21

Rianjanu, A., T. Haloho, J. L. Pasaribu, A. G. Fahmi, E. Nurfani, W. S. Sipahutar, H. T. Yudistira, and T. Taher (2025). Electrospun Rare-Earth Metal Oxide (CeO_2) Nanofiber for the Degradation of Congo Red Aqueous Dyes. *Science & Technology Indonesia*, **10**(1); 123–130

Sagadevan, S., J. A. Lett, and I. Fatimah (2023). One-Pot Hydrothermal Synthesis and Characterization of Zirconium Oxide Nanoparticles. *Science & Technology Indonesia*, **8**(4); 585–593

Shi, X., Y. Chen, G. Li, K. Qiang, Q. Mao, L. Pei, M. Liu, and J. Zhong (2023). Designing a Dual-Wavelength Excitation Eu^{3+}/Mn^{4+} Co-Doped Phosphors for High-Sensitivity Luminescence Thermometry. *Ceramics International*, **49**(12); 20839–20848

Tang, Q., N. Guo, Y. Xin, W. Li, B. Shao, and R. Ouyang (2021). Luminous Tuning in Eu^{3+}/Mn^{4+} Co-Doped Double Perovskite Structure by Designing the Site-Occupancy Strategy for Solid-State Lighting and Optical Temperature Sensing. *Materials Research Bulletin*, **149**; 111704

That, P. T. and N. D. Q. Anh (2021). Green $Ca_2La_2BO_6 \cdot {}_5$:Pb_2^+ Phosphor: An Innovative Solution in Enhancing the Color Quality and Luminous Flux of WLEDs. *TELKOMNIKA (Telecommunication Computing Electronics and Control)*, **19**(5); 1630

Thuy, L. X., H. T. Tung, L. T. Dat, and N. L. M. Nhan (2025). Performance of ZnS and ZnSe Doped on Cu^{2+} for Photovoltaic Devices. *Science & Technology Indonesia*, **10**(3); 952–957

Tung, H. T., N. T. P. Loan, and N. D. Q. Anh (2024a). The Enhancement Chromatic Uniformity and Illuminating Flux of WLEDs with Dual-Layer Phosphorus Configuration. In *Lecture Notes in Electrical Engineering*. pages 167–174

Tung, H. T., B. T. Minh, N. L. Thai, H. Y. Lee, and N. D. Q. Anh (2024b). ZnO Particles as Scattering Centers to Optimize Color Production and Lumen Efficiencies of Warm White LEDs. *Optoelectronics and Advanced Materials - Rapid Communications*, **18**(5–6); 1–6

